ARTICLE

X-ray and DFT Study of Glaucocalyxin A Compound with Cytotoxic Activity

Fu-dong Wang[a,f], Tao Wang[b,e], An-an Wu[c], Lan Ding[d], Han-qing Wang[a*]

a. State Key Laboratory of Solid Lubrication, Lanzhou Institute of Chemical Physics, Chinese Academy of Sciences, Lanzhou 730000, China
b. Collage of Physics and Mechanical Electrical Engineering, Xiamen University, Xiamen 361005, China
c. State Key Laboratory of Physical Chemistry of Solid Surfaces, Collage of Chemistry and Chemical Engineering, Xiamen University, Xiamen 361005, China
d. College of Life Science, Northwest Normal University, Lanzhou 730070, China
e. Department of Chemistry and Chemical Engineering, Heze University, Heze 274015, China
f. Graduate School of the Chinese Academy of Sciences, Beijing 100039, China

(Dated: Received on November 2, 2008; Accepted on December 22, 2008)

The title compound glaucocalyxin A (**1**) (7α,14β-dihydroxy-ent-kaur-16-en-3,15-dione) isolated from the leaves of *isodon excisoides* was characterized by IR, ^{1}H NMR, ^{13}C NMR, ^{1}H-^{1}H COSY, HMQC, HMBC, and EIMS, and its crystal structure was determined by single-crystal X-ray diffraction. The X-ray crystal structure revealed that the molecular backbone of the chosen crystal is a tetracyclic system, including three six-membered rings and a five-membered ring, and the three six-membered rings are in a chair-like conformation. The five-membered ring adopts a twisted envelope-like conformation, and its geometrical parameters were compared with theoretical calculations at the B3LYP and HF level of theory. The molecules form extensive networks through the intra- and intermolecular hydrogen bonds. The experimental NMR data were interpreted with the aid of magnetic shielding constant calculations, by means of the GIAO (gauge-lncluding atomic orbitals) method. Calculated and experimental results were compared with a satisfactory level of agreement. Molecular electrostatic potential map was used in an attempt to identify key features of the diterpenoid glaucocalyxin A that is necessary for its activity. Calculations of molecular electrostatic potential and stabilization energies suggest that the protonation of glaucocalyxin A will be able to occur on carbonyl oxygen atoms.

Key words: *Isodon excisoides*, Glaucocalyxin A, X-ray structure, Density functional theory

I. INTRODUCTION

Diterpenoids are widely spread in plants, especially in *isodon*. More than 400 ent-kaurane diterpenoids have been found from the genus *isodon* [1]. The diterpenoids constituents of *isodon* plants have attracted chemists and pharmacologists for a long time because of their structure diversity and significant biological activities, such as anticancer, anti-inflammatory, and antiviral activities. *Isodon excisoides* has been used in Chinese folk medicine to treat gastric ulcers and enteritis, and is distributed in the south of Gansu province and Yunnan province, China. Pharmacological research has proved that the biological activities of the compounds are intensely associated with their conformation features and key functional groups. It is highly important in pharmacology to establish the accurate molecular configuration by single-crystal X-ray diffraction. Elucidation of their structure have shown some interesting features which required additional studies. Therefore, the reports on the X-ray structural determination, quantum chemical calculation and spectroscopic study of the compounds are meaningful.

Isodon excisoides (Sun ex C. H. Hu) C. Y. Wu et H. W. Li is distributed in northeast of Gansu province in China. However, the activity component about this plant is rare reported [2]. To find new bioactive substance, we investigated the chemical components of this plant collected from Gansu province, China, and isolated twelve compounds in which diterpenoids glaucocalyxin A (**1**) was obtained as crystals. Although the compound has been isolated previously from other *isodon* species [3], this is the first time it was obtained from *isodon excisoides* (Sun ex C. H. Hu) C. Y. Wu et H. W. Li, and no crystallographic data have been available till now. Recently, our pharmacological research indicated that compound **1** shows the most significant cytotoxicity activity [4,5].

*Author to whom correspondence should be addressed. E-mail: whqwt@yahoo.com.cn

Nuclear magnetic resonance (NMR) spectroscopy constitutes an extremely useful tool for the determination of molecular electronic structure and molecular conformation. Calculations of NMR chemical shifts at various level of theory have become a standard method in chemistry [6-8]. Because of the sensitivity to the electronic structure in their environment, magnetically active nuclei can be used to probe the near-by shielding influences. This is one of reasons why NMR spectroscopy rivals X-ray diffraction as the most important experimental tool for characterizing molecular structure [9]. The assignment of the chemical shifts to different magnetic nuclei in molecular investigation is an important task for NMR spectroscopy. Quantum chemical calculations may be able to provide valuable support for experimental results, and provide a very important source of information allowing us to obtain both the molecular geometry and the NMR chemical shifts values. Many efforts have been devoted to the calculation of NMR chemical shifts in order to carry out a correct assignment of the experimental data [10]. For this reason it has received a great deal of attention from the theoretical chemists and NMR spectroscopists for many years.

Recently the gauge including atomic orbital (GIAO) [11,12] method for calculation of NMR chemical shifts has become a standard and has been implemented in major quantum chemistry packages. The GIAO method facilitates accurate NMR chemical shift calculations via electron-correlation methods. Theoretical calculations coupled with the GIAO calculations have been employed to help the NMR assignment of the investigated compound [13]. The theoretical methods, such as density functional theory (DFT) method have become the dominant computational tools for dealing with natural products [14,15].

The electrostatic potential created in the space around a molecule by its nuclei and electrons is well established as a guide to molecular reactive behavior. In recent years, surface molecular electrostatic potentials (MEP) [16] have been used extensively as a tool for identifying and ranking the molecular regions most susceptible to electrophilic and nucleophilic attack and for determining general patterns of positive and negative potential that promote or inhibit molecular interaction, such as those between drug and receptor. Thus electrostatic properties might be indicative of a match between the receptor site and the particular molecule.

In this work, X-ray crystalline structure and NMR experimental results for compound **1** are presented and compared with theoretical calculations carried out with DFT method. A comparison of the experimental and theoretical values can be very useful in making correct assignments and understanding the basic chemical shifts-molecular structure relationship, so these calculations are valuable for providing insight into the molecular structure. In this research, MEP maps were used in an attempt to identify the key moiety of compound **1** that is necessary for its biological activity.

II. EXPERIMENTS

A. Instruments

Melting point of compound **1** was obtained on Kofler-microscope (Reichert) apparatus and is uncorrected. IR spectra were recorded on an IFS-120HR (Germany) IR spectrophotometer with KBr pellets. ^{1}H and ^{13}C NMR spectra were performed on a Varian INOVA-400 spectrometer by using $CDCl_3$ as solvent and TMS as an internal standard (chemical shift in ppm). ^{1}H and ^{13}C NMR assignments were supported by ^{1}H-^{1}H COSY, HMQC, and HMBC experiments; EIMS was measured on a VG-ZAB-HS mass spectrometer.

B. Plant material

The leaves of *isodon excisoides* were collected in August 2003 from Zhangxian, Gansu province, China. The plant was identified by Prof. Kun Sun and a voucher specimen was deposited in the College of Life Science, Northwest Normal University, China.

C. Extraction and isolation

The air-dried and powdered plants (5.0 kg) were extracted with 95% ethanol at room temperature three times. The concentrated extract was partitioned between water and EtOAC. The EtOAC extract (100 g) was introduced onto a silica gel column and eluted with $CHCl_3$-acetone (100:1-1:100) to obtain the title compound in a yield of 30 mg. The compound crystallized as colorless crystals ($CHCl_3$). The molecular formula, $C_{20}H_{28}O_4$, was established by EIMS (m/z 332, M^+, 100); mp: 224-226 °C; IR (KBr): 3244, 2965, 2940, 2869, 1726, 1708, and 1652 cm^{-1}.

D. Crystallographic data collection and structure determination

A colorless platelet single crystal with approximate dimensions of 0.49 mm×0.49 mm×0.34 mm was mounted on a glass fiber. X-ray diffraction intensity data were collected on a Rigaku R-Axis Rapid IP detector equipped with a graphite monochromated MoKα radiation (λ=0.71073 Å) by using a ω scan mode at 293 K. A total of 14473 reflections were collected within $1.68° \leq \theta \leq 27.63°$, of which 2290 unique reflections ($R_{\rm int}$=0.0417) and 2290 observed reflections with $I \geq 2\sigma(I)$ were used in the succeeding structure determination and refinements. The crystal structure was solved by direct methods using the SHELXSTL$^{\rm TM}$ version 5 package of crystallographic software [17] and re-

DOI:10.1088/1674-0068/22/03/275-284

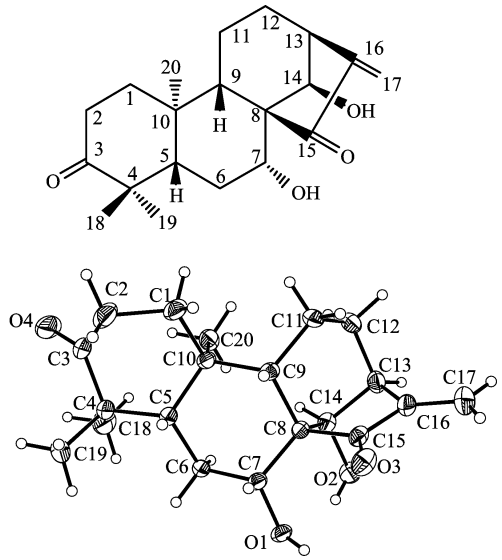

FIG. 1 In plane and ORTEP (30% ellipsoid probability) representations of compound **1**.

fined by full-matrix least-squares refinement on F^2. All non-hydrogen atoms were refined anisotropically. The hydrogen atoms were generated symmetrically, allowed to ride on their respective parent atoms and included in the structure factor calculations with assigned isotropic thermal parameters, but not refined. The final refinement converged at R=0.0424, wR=0.1233, S=1.003. The largest peak and deepest hole on the final difference Fourier map were 0.187 and −0.262 e/Å^3, respectively. Obtained X-ray structures and its crystal packing are displayed in Fig.1. Table I shows a summary of data collection and refinement conditions of the crystal structure.

TABLE I Crystal and structure refinement data for compound **1**.

Empirical formula	$C_{20}H_{28}O_4$
Formula weight	332.42
Wavelength (MoKα)	0.71073 Å
Crystal system	Orthorhombic
Space group	P2(1)2(1)2(1)
Unit cell dimensions	a=6.6454(13) Å, α=90°
	b=10.650(2) Å, β=90°
	c=24.264(5) Å, γ=90°
Volume	1717.3(6) Å^3
Z	4
Calculated density	1.286 mg/m^3
Absorption coefficient	0.088 mm^{-1}
F(000)	720
Crystal size	0.49 mm×0.49 mm×
	0.34 mm
θ for data collection	1.68°-27.63°
Limiting indices	$-8\leq h\leq 8$, $-12\leq k\leq 13$,
	$-30\leq l\leq 31$
Reflections collected/unique	14473/2290
	$R_{\rm int}$=0.0417
Completeness to θ=27.63°	98.9%
Absorption correction	Empirical
Max. and min. transmission	0.9704 and 0.9581
Refinement method	Full-matrix least-squares
	on F^2
Data/restraints/parameters	2290/0/217
Goodness-of-fit on F^2	1.003
Final R indices [I>2σ(I)]	$R1$=0.0424, $wR2$=0.1233
R indices (all data)	$R1$=0.0484, $wR2$=0.1302
Absolute structure parameter	−1.1(15)
Largest diff. peak and hole	0.187 and −0.262 e/Å^3

E. Computational methods

Because of the large number of possible conformations for compound **1**, in this study the geometry obtained from X-ray diffraction was used as input for the full geometry optimization via the HF and B3LYP hybrid functional [18,19], together with the 6-31G(d,p) basis set. Each optimization was followed by frequency calculations to test whether the optimal points are true minima or just saddle points. NMR (^{1}H and ^{13}C chemical shifts) spectra were calculated by B3LYP level. The 6-31G(d,p) and 6-311G(d,p) basis sets augmented with diffuse and polarization functions were used at geometries optimized with the B3LYP/6-31G(d,p) method, using GIAO approximation. In order to compare isotropic shielding with experimental chemical shifts, the NMR parameters for reference molecule tetramethylsilane (TMS) were calculated at the same level of theory. All calculations were performed with the Gaussian 03 program package [20]. The surface molecular electrostatic potential (MEP) was generated from the B3LYP/6-31G(d,p) with the geometry optimized in B3LYP/6-31G(d,p). Electrostatic mapping on the density surface was performed using the Chemoffice program.

F. Regression analysis

The NMR data were analyzed for linear regression and relevant parameters were selected: the correlation coefficients R and standard deviation SD. In additional, other statistical parameters were available to judge the quality of a calculation. For each system we present the parameters a and b of the linear regression

$$\delta_{\rm calc.} = a + b\delta_{\rm expt.} \quad (1)$$

and the mean absolute error (MAE) defined as

$$MAE = \sum_n \frac{1}{n}|\delta_{\rm calc.} - \delta_{\rm expt.}| \quad (2)$$

DOI:10.1088/1674-0068/22/03/275-284

TABLE II Atomic coordinates ($\times 10^4$) and equivalent isotropic displacement parameters (10^3 Å).

Atom	x	y	z	U(eq)	Atom	x	y	z	U(eq)
O(1)	1850(2)	8926(1)	−40(1)	39(1)	C(9)	1463(3)	9475(2)	1497(1)	32(1)
O(2)	3276(3)	6952(1)	479(1)	44(1)	C(10)	3053(3)	10541(2)	1563(1)	33(1)
O(3)	−1985(2)	8252(2)	785(1)	48(1)	C(11)	1274(4)	8600(2)	2004(1)	44(1)
O(4)	6066(4)	13572(2)	1797(1)	83(1)	C(12)	2452(4)	7377(2)	1976(1)	48(1)
C(1)	2270(4)	11423(2)	2023(1)	50(1)	C(13)	2242(3)	6747(2)	1413(1)	42(1)
C(2)	2770(5)	12807(2)	1941(1)	62(1)	C(14)	3149(3)	7633(2)	985(1)	34(1)
C(3)	4639(5)	13002(2)	1619(1)	52(1)	C(15)	−378(3)	7902(2)	961(1)	34(1)
C(4)	4627(4)	12447(2)	1041(1)	44(1)	C(16)	70(3)	6691(2)	1241(1)	42(1)
C(5)	3142(3)	11311(2)	1025(1)	33(1)	C(17)	−1287(5)	5812(3)	1321(1)	66(1)
C(6)	3402(3)	10477(2)	522(1)	34(1)	C(18)	6787(5)	12140(3)	864(1)	65(1)
C(7)	1648(3)	9582(2)	469(1)	31(1)	C(19)	3846(6)	13495(2)	672(1)	69(1)
C(8)	1565(3)	8682(2)	957(1)	28(1)	C(20)	5132(3)	10064(2)	1740(1)	45(1)

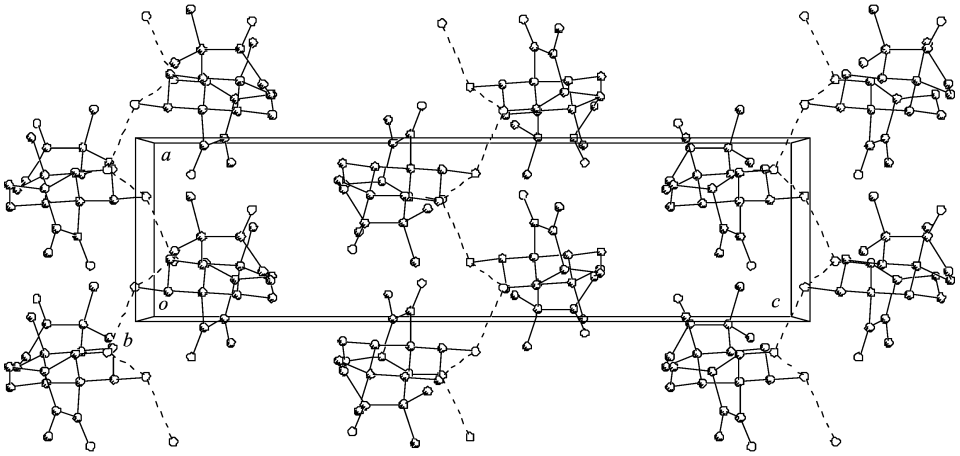

FIG. 2 Packing diagram of the title compound with the dashed lines representing the hydrogen bonds.

III. RESULTS AND DISCUSSION

A. X-ray crystallographic and DFT structure

The single crystal X-ray diffraction analysis of compound **1** revealed that the molecular backbone of the chosen crystal is a tetracyclic system, including three six-membered rings and a five-membered ring. The six-membered rings are in a chair-like conformation and the five-membered ring adopts a twisted envelope-like conformation, as shown in Fig.1.

An ORTEP drawing of compound **1** showing the molecular conformation and atom-labeling is depicted in Fig.1. The atomic coordinates and equivalent thermal parameters for non-hydrogen atoms are listed in Table II.

The X-ray crystal structure showed that the hydroxyl group at C7 was in the α-orientation, the hydroxyl at C14 in the β-orientation, and the carbonyl group at C3. Thus, the structure of the title compound was elucidated to be 7α,14β-dihydroxyl-ent-kaur-16-en-3,15-dione.

The glaucocalyxin A (**1**) molecules interlinked to each other via intermolecular O1($x-1/2$, $-y+3/2$, $-z$)$\cdots$O2 hydrogen bond with a distance of 2.766(2) Å and intramolecular O1$\cdots$O2 hydrogen bond with a distance of 2.628(2) Å to construct the supramolecular infinite chain running along a axis. The chains are arranged in parallel to form a 3D structure only via van de Waals' force, as shown in Fig.2 and Table III.

Table IV lists selected bond lengths and angles calculated for compound **1**, along with parameters reported from X-ray diffraction analysis of compound **1**. They were obtained from the HF/6-31G(d,p) and B3LYP/6-31G(d,p) level. Figure 3 shows the geometry of molecule compound **1** obtained by B3LYP/6-31G(d,p). From the Table IV, a good agreement is seen between theoretical and experimental values.

B. NMR spectra and their evaluation by theory methods

We successfully carried out the assignment of the NMR spectra of compound **1** using a combination of

DOI:10.1088/1674-0068/22/03/275-284

TABLE III Hydrogen bond lengths and bond angles.

D−H···A	Hydrogen bond length/Å			Bond angle/(°)
	D−H	H···A	D−H···A	
O(1)−H(1 A)···O(2)[a]	0.82	1.95	2.766(2)	172.3
O(2)−H(2 A)···O(1)	0.82	1.88	2.628(2)	150.9
O(2)−H(2 A)···O(3)[b]	0.82	2.55	3.079(2)	123.7

[a] Symmetry operator: $x-1/2$, $-y+3/2$, $-z$.
[b] Symmetry operator: $x+1/2$, $-y+3/2$, $-z$.

TABLE IV Selected bond lengths (in Å) and bond angles (in (°)) for compound **1**: the theoretical calculations and X-ray structure.

Parameter	Bond	Exp.(X-ray)	HF/6-31G(d,p)	B3LYP/6-31G(d,p)
Bond lengths/Å	O(1)−C(7)	1.423(4)	1.411	1.439
	O(3)−C(15)	1.209(3)	1.194	1.220
	O(4)−C(3)	1.206(3)	1.193	1.217
	C(1)−C(2)	1.524(4)	1.544	1.551
	C(4)−C(18)	1.534(4)	1.543	1.553
	C(4)−C(5)	1.562(3)	1.560	1.571
	C(5)−C(10)	1.543(2)	1.564	1.567
	C(8)−C(15)	1.536(2)	1.537	1.547
	C(8)−C(9)	1.561(2)	1.565	1.575
	C(9)−C(10)	1.559(3)	1.575	1.5793
	C(12)−C(13)	1.528(3)	1.531	1.542
	C(16)−C(17)	1.314(3)	1.314	1.334
Bond angles/(°)	O(4)−C(3)−C(2)	122.7(2)	112.1	122.4
	O(4)−C(3)−C(4)	122.0(2)	112.4	122.3
	C(3)−C(4)−C(18)	109.7(2)	109.8	115.1
	C(3)−C(4)−C(5)	109.1(16)	109.4	109.6
	C(6)−C(5)−C(4)	113.6(15)	112.7	112.7
	C(10)−C(5)−C(4)	114.5(15)	114.9	114.6
	C(6)−C(7)−C(8)	111.0(14)	112.2	112.3
	C(14)−C(8)−C(9)	112.6(14)	111.9	112.2
	C(10)−C(9)−C(8)	116.8(13)	116.3	116.0
	C(20)−C(10)−C(5)	112.2(16)	112.1	112.0
	C(5)−C(10)−C(9)	109.0(14)	108.6	108.8
	C(11)−C(12)−C(13)	111.7(17)	111.6	111.5
	O(2)−C(14)−C(13)	107.1(15)	107.0	107.5
	O(2)−C(14)−C(8)	111.8(15)	112.7	112.2
	O(3)−C(15)−C(8)	125.0(19)	125.1	124.9
	C(17)−C(16)−C(15)	123.2(2)	123.0	122.9
Dihedral angles/(°)	C(10)−C(1)−C(2)−C(3)	−25.3	−26.2	−25.2
	C(2)−C(1)−C(10)−C(5)	−28.8	−29.7	−31.1
	C(1)−C(2)−C(3)−C(4)	59.6	59.3	59.0
	C(3)−C(4)−C(5)−C(10)	−34.4	−32.1	−31.8
	C(4)−C(5)−C(6)−C(7)	−169.3	169.4	−169.4
	C(4)−C(5)−C(10)−C(9)	178.1	177.6	178.2
	C(6)−C(5)−C(10)−C(1)	−166.3	−167.5	−167.1
	C(5)−C(6)−C(7)−C(8)	−61.9	−62.1	−61.9
	C(7)−C(8)−C(9)−C(10)	−50.7	−50.5	50.7
	C(15)−C(8)−C(9)−C(11)	56.5	56.6	56.5
	C(9)−C(8)−C(14)−O(3)	71.7	72.6	71.3
	C(14)−C(13)−C(16)−C(15)	−27.9	−27.0	−26.8

DOI:10.1088/1674-0068/22/03/275-284

TABLE V Theoretically predicted and experimentally observed ^{1}H-NMR (in ppm) of compound **1** which was optimized geometry at B3LYP/6-31G(d,p) level.

C	Exp.	6-31G(d,p)	$\triangle\delta$	6-31+G(2d,p)	$\triangle\delta$	6-311G(d,p)	$\triangle\delta$	6-311+G(2d,p)	$\triangle\delta$
1	1.40	1.37	−0.03	1.32	−0.08	1.41	0.01	1.38	−0.02
	1.70	1.77	0.07	1.73	0.03	1.73	0.03	1.77	0.07
2	2.58	2.64	0.06	2.70	0.12	2.70	0.12	2.70	0.12
	1.99	1.95	−0.04	2.00	0.01	2.02	0.03	2.04	0.05
5	1.92	1.95	0.03	1.86	−0.06	1.81	−0.11	1.86	−0.06
6	1.85	1.90	0.05	1.91	0.06	1.97	0.12	1.93	0.08
	1.70	1.85	0.15	1.68	−0.02	1.75	0.05	1.67	−0.03
7	4.63	4.41	−0.22	4.46	−0.17	4.40	−0.23	4.84	0.21
9	1.37	1.36	−0.01	1.14	−0.23	1.18	−0.19	1.26	−0.11
11	1.40	1.49	0.09	1.30	−0.10	1.30	−0.10	1.32	−0.08
	1.55	1.50	−0.05	1.50	-0.05	1.49	−0.06	1.49	−0.06
12	1.68	1.66	−0.02	1.70	0.02	1.68	0.00	1.77	0.09
	1.97	1.90	−0.07	1.93	−0.04	1.93	−0.04	1.94	−0.03
13	3.11	2.98	−0.13	3.05	−0.06	2.96	−0.15	3.07	−0.04
14	4.85	4.76	−0.09	4.84	−0.01	4.69	−0.16	4.90	0.05
17	6.18	6.52	0.34	6.56	0.38	6.59	0.41	6.50	0.32
	5.43	5.43	0.00	5.43	0.00	5.50	0.07	5.46	0.03
18-CH_3	1.04	1.10	−0.06	1.01	−0.03	1.11	0.07	1.10	0.06
19-CH_3	1.10	1.07	−0.03	1.07	−0.03	1.25	0.15	0.94	−0.16
20-CH_3	1.09	0.99	−0.10	1.02	−0.07	0.84	−0.25	0.87	−0.22
OH	4.85	4.75	−0.10	5.11	0.26	4.59	−0.26	4.79	−0.06
TMS		31.71		31.59		31.92		31.82	

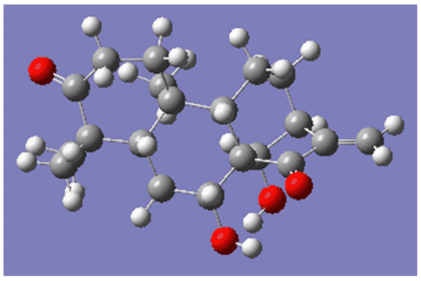

FIG. 3 Optimized structure of compound **1** determined at B3LYP/6-31G(d,p) level. Colored atom: oxygen (in red), carbon (in grey) and hydrogen (in white). For interpretation of the color in this figure legend, the reader can refer to the web version of this article.

1D and 2D NMR spectroscopic techniques together with the use of DFT calculations for isolated molecules. Although there is some overlap of resonances in the NMR spectra of compound **1**, all of ^{1}H and ^{13}C NMR data could be assigned by a combination of DEPT, ^{1}H-^{1}H COSY, HMQC, HMBC, and quantum chemical calculation.

The NMR spectra indicated the presence of three methyls, six methylenes (including an exomethylene), five methines (two of which were oxygenated), and six quaternary carbons (including two carbonyl carbons). In addition, the partial structure of an exomethylene conjugated with a carbonyl group on a five-membered ring was revealed by its NMR (δ_C at 207.5(s), 147.1(s), 118.4(t); δ_H at 6.18(1H,s), 5.43(1H,s)), which corresponded to the basic skeleton of ent-kaurane diterpenoids previously described in the genus *isodon* [21-24].

The typical ^{1}H and ^{13}C NMR signals of compound **1** at δ_H 3.54(1H,dd) and δ_H 4.85(1H,s) and at δ_C 74.2(d), δ_C 74.8(d), and δ_C 216.7(s) established the presence of two hydroxyl groups and a carbonyl group. The aforementioned inferences were confirmed by an X-ray diffraction analysis. The cross-peaks observed in the HMBC revealed that two hydroxyl groups were located at C7 and C14. The aforementioned inference was confirmed by X-ray diffraction analysis.

The ^{1}H and ^{13}C NMR chemical shifts were calculated for compound **1** and TMS (internal standard) using B3LYP methods. The experimental and calculated ^{1}H and ^{13}C chemical shifts are shown in Tables V and VI. The chemical shifts were obtained by subtracting the calculated magnetic shielding for the nuclei of interest from the reference compound shielding (TMS for ^{1}H and ^{13}C). Figure 4 show the correlation between the calculated and experimental data of ^{1}H and ^{13}C chemical shifts. From the statistical analysis, it can be seen that all models for ^{1}H and ^{13}C chemical shifts show a good

DOI:10.1088/1674-0068/22/03/275-284

TABLE VI Predicted and experimental ^{13}C NMR chemical shifts (in ppm) of compound **1** which was optimized geometry at B3LYP/6-31G(d,p) level of theory.

	Exp.	6-31G(d,p)	$\triangle\delta$	6-31+G(2d,p)	$\triangle\delta$	6-311G(d,p)	$\triangle\delta$	6-311+G(2d,p)	$\triangle\delta$
C(1)	38.1	41.8	3.7	42.1	4.0	44.4	6.3	44.0	5.9
C(2)	33.6	33.2	−0.4	35.1	1.5	37.0	3.4	36.4	2.8
C(3)	216.7	208.9	−7.8	214.2	−2.5	223.8	7.1	226.3	9.6
C(4)	46.7	49.7	3.0	48.7	2.0	52.7	6.0	54.9	8.2
C(5)	51.6	51.8	0.2	53.1	1.5	56.5	4.9	56.1	4.5
C(6)	28.9	29.6	0.7	30.2	1.3	31.7	2.8	30.3	1.4
C(7)	74.2	75.9	1.7	76.4	2.2	81.2	7.0	81.8	7.6
C(8)	61.5	64.1	2.6	65.1	3.6	68.8	7.3	68.3	6.8
C(9)	52.6	55.0	2.4	55.7	3.1	59.4	6.8	58.7	6.1
C(10)	38.7	42.8	4.1	44.3	5.6	46.4	7.7	45.9	7.2
C(11)	18.1	21.5	3.4	22.8	4.7	23.6	5.5	23.0	4.9
C(12)	30.8	32.8	2.0	34.3	3.5	35.9	5.1	35.8	5.0
C(13)	45.8	48.3	2.5	50.1	4.3	52.6	6.8	52.9	7.1
C(14)	74.8	76.3	1.5	76.4	1.6	81.1	6.3	81.0	6.2
C(15)	207.5	203.8	−3.7	207.5	0.0	218.0	10.5	218.8	11.3
C(16)	147.1	145.0	−2.1	147.7	0.6	158.7	11.6	158.4	11.3
C(17)	118.4	115.7	−2.7	116.8	−1.6	124.5	6.1	124.0	5.6
C(18)	20.9	21.3	0.4	20.6	−0.3	21.6	0.7	20.7	−0.2
C(19)	27.7	29.2	1.5	29.6	1.9	30.9	3.2	30.2	2.5
C(20)	18.3	22.0	3.7	22.7	4.4	23.0	4.7	21.5	3.2
TMS		191.5		191.0		183.8		182.5	

linear correlation, as indicated by the high correlation coefficients (R>0.99). The best results were observed at the B3LYP/6-31(d,p) and B3LYP/6-31+G(d,p) level of theory.

Calculations of ^{13}C chemical shifts using B3LYP methods with triple split-valence basis sets gave larger errors than the corresponding methods with double split-valence basis sets. Moreover, augmentation of the triple split-valence basis sets with additional polarization and diffuse functions led to an overestimation of ^{13}C chemical shifts at the B3LYP level of theory. More accurate values of ^{13}C chemical shifts were obtained from the calculations using double split-valence basis sets.

C. MEP and drug activities

Figure 5 shows the three-dimension MEP surface of compound **1**. In Fig.5, one can see that the lowest electronic potential can be found in the proximity of the oxygen atoms of carbonyl oxygen (O3 and O4 groups). The large negative potential (in blue) on the oxygen atoms may be regarded as a nucleophilic suction pump [14,25], acting as a possible magnet for the electrophilic attack of H^+ or part of a biological receptor. The rest of the molecule presents a low positive potential, stronger near the hydrogen positions. Therefore, calculations were carried out for the protonation on the O3 and O4 (carbonyl oxygen) positions of compound **1**. Table VII presents free energies of compound **1** in gas phase and in water. The relative energies found were −864.8(−1120.7) kJ/mol for protonation on position O3 and −855.6 (−1108.1) kJ/mol for protonation on position O4 (values in parenthesis are for protonation energy in water). For the O3 and O4 positions, the difference between O3/O4 energies is 9.2(12.5) kJ/mol, i.e., the protonation occurs preferentially on the O3 atom. The protonation in O3 is favored probably by the increase of the electronic density in this oxygen due to the effect of resonance generated for the conjugation of carbonyl of ketone with a α-methylene on a five-membered ring. This might imply that the α-methylene cyclopentanone moiety for compound **1** plays a dominant role in the biological activity of this molecule. While the region with more positive electronic potential (in henna) is around the hydrogen and carbon atoms, The protoned species have low permeability coefficient across membranes and might react covalently with free sulfhydryl groups on the extracellular surface of the H^+, K^+-ATPase [23,26].

From the Table VII, one can see that the energies of protonation on the oxygen atomic sites in aqueous media are appreciably larger than those in gas phase. This is due to an appreciable modification of charge distribution in going from the gas phase to aqueous.

DOI:10.1088/1674-0068/22/03/275-284

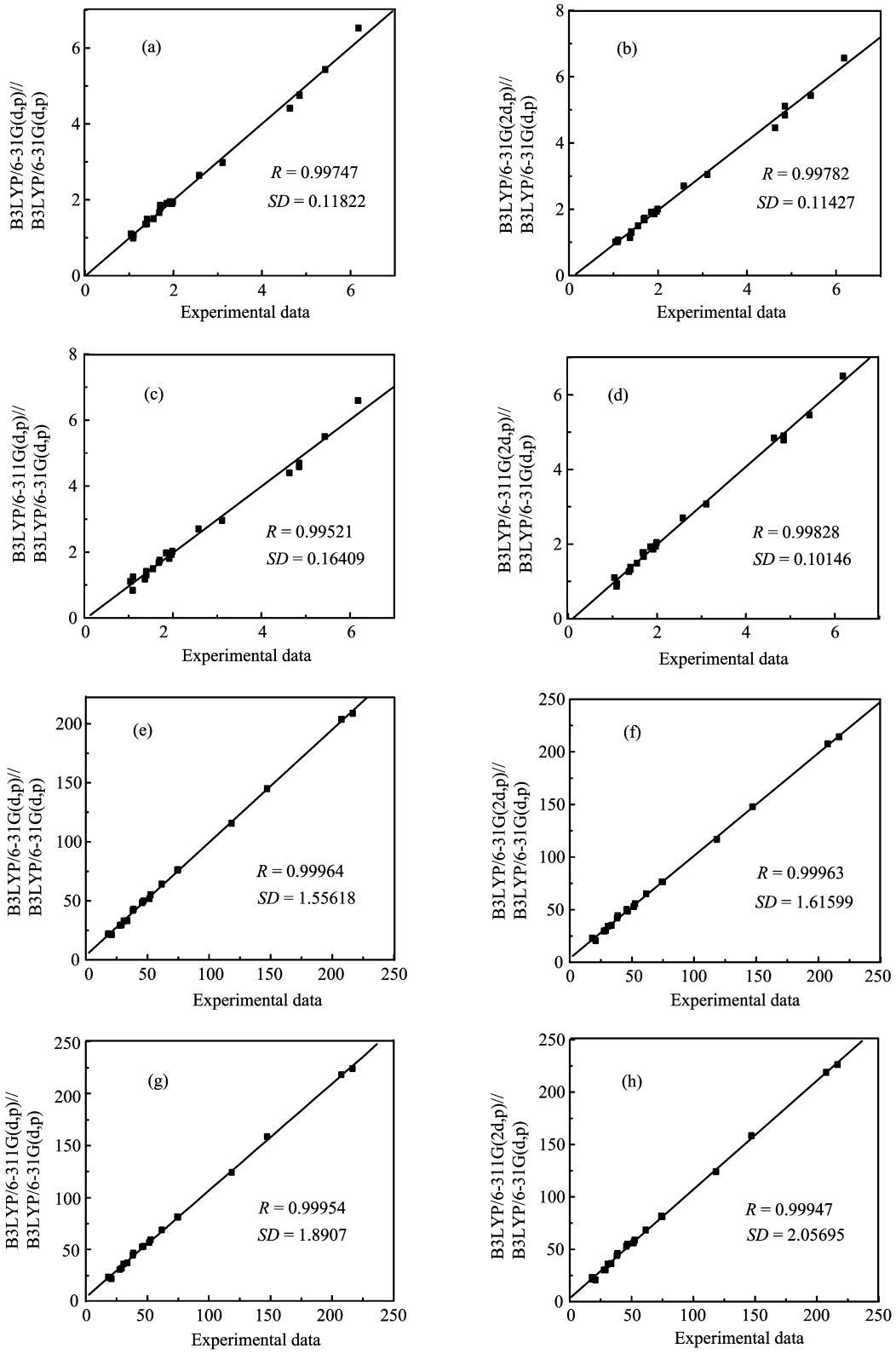

FIG. 4 The linear regression between experimental and GIAO calculated NMR chemical shifts (in ppm) for compound **1**, (a)-(d) ^{1}H NMR, (e)-(h) ^{13}C NMR.

DOI:10.1088/1674-0068/22/03/275-284

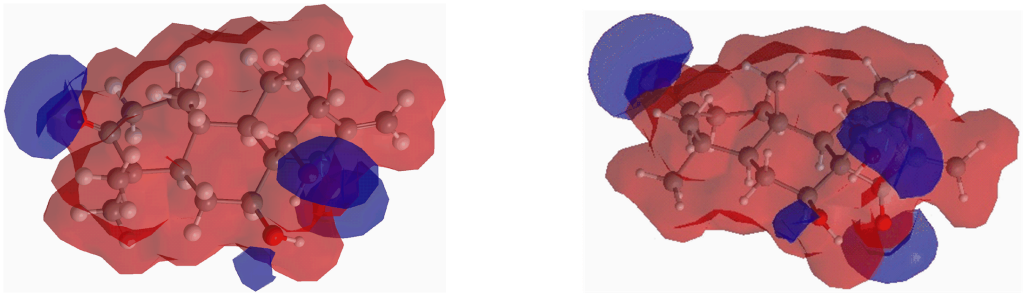

(a) (b)

FIG. 5 Three-dimensional MEP of compound **1** derived from B3LYP/6-31G(d,p) calculation in gas phase (a) and in water (b). The colored blue and henna present negative and positive electronic potential, respectively. For interpretation of the color in this figure legend, the reader can refer to the web version of this article.

TABLE VII The energies of protonation for compound **1** on O3 and O4 positions calculated on the 6-31G(d,p) basis set.

	E/Hartree	ZPE/Hartree	E+ZPE/Hartree	PA/Hartree	PA/(kJ/mol)
Glaucocalyxin A	−1079.931	0.477426	−1079.45405		
Protoned on O3 (gas)	−1080.273	0.489508	−1079.78371	0.3296645	−864.8
Protoned on O4 (gas)	−1080.270	0.489665	−1079.78030	0.3262508	−855.6
Protoned on O3 (water)	−1080.344	0.462899	−1079.88132	0.4272739	−1120.7
Protoned on O4 (water)	−1080.339	0.462647	−1079.87659	0.4225416	−1108.1

IV. CONCLUSION

The X-ray and NMR experimental results for compound **1** are presented and compared with quantum chemical calculations carried out with DFT methods. Compound **1** has the basic skeleton of 7α,14-dihydroxy-ent-kaur-16-en-3,15-dione and its structure was confirmed by crystallographic analysis. The predicted geometric parameters for compound **1** are close to the X-ray crystal structure. NMR theoretical values obtained with all basis sets shows good correlations and high predictive power. Therefore, DFT (B3LYP) calculations can attain a considerable degree of accuracy in the prediction of the ^{1}H and ^{13}C NMR spectra of naturally occurring organic molecules. Our MEP results show that the α-methylene cyclopentanone moiety for compound **1** plays a dominant role in the biological activity of this molecule. The MEP surface of compound **1** shows two sites susceptible to protonation (O3 and O4 positions). Calculations of molecular electrostatial potential and stabilization energies suggest that protonation of compound **1** occurs preferentially on O3 oxygen atom (carbonyl oxygen on cyclopentanone). The protoned species might improve the interaction with the extracellular surface of the H^+, K^+-ATPase.

V. ACKNOWLEDGMENT

This work was supported by the State Key Laboratory for Physical Chemistry of Solid Surface, Xiamen University.

[1] H. D. Sun. Y. L. Xu, and B. Jiang, *Diterpenoids from* isodon *Species*, Beijing: Science Press, 111 (2001).
[2] L. Ding, H. Wang, G. A. Liu, and D. J. Yang, J. Chem. Res. 697 (2004).
[3] Y. L. Xu, X. C. Sun, and H. D. Sun, Acta Bot. Yunnaica **3**, 283 (1981).
[4] L. Ding, Z. J. Zhang, G. A. Liu, D. J. Yang, G. C. Guo, H. Wang, and K. Sun, Z. Naturforsch. **60**, 805 (2005).
[5] G. A. Liu, L. Ding, Y. Yang, H. Yang, Q. M. Yang, and H. Q. Wang, Res. Chem. Intermed. **32**, 787 (2006).
[6] M. Bühl, M. Kaupp, O. L. Malkina, and V. G. Malkin, J. Comput. Chem. **91**, 20 (1999)
[7] Z. Schreckenbach and T. Ziegler, Theor. Chem. Acc. **99**, 71 (1998).
[8] B. Wang, U. Fleischer, J. F. Hinton, and P. Pulay, J. Comput. Chem. **22**, 1887 (2001).
[9] H. Gunther, *NMR Spectroscopy: Basic Principles, Concepts, and Applications in Chemistry*, 2nd edn., New York: Wiley and Sons, (1995).
[10] M. Barfield and R. Fagerness, J. Am. Chem. Soc. **119**, 8699 (1997).
[11] R. Dithchfield, J. Chem. Phys. **56**, 5688 (1972)
[12] K. Wolinski, J. F. Hinton, and P. Pulay, J. Am. Chem. Soc. **112**, 825 (1990)
[13] M. Dincer, D. Maci, M. Sekerci, and Y. Atalay, J. Mol. Model. **14**, 823 (2008)
[14] D. S. B. Brasil, R. Y. O. Moreira, A. H. Muller, and C. N. Alves, Int. J. Quantum Chem. **106**, 2706 (2006).
[15] D. S. B. Brasil, C. N. Alves, G. M. S. P. Guilhon, A. H. Muller, R. de S. Secco, G. Peris, and R. Llusar, Int. J. Quantum Chem. **108**, 2564 (2008).
[16] F. J. B. Cardoso, A. F. de Figueiredo, M. da Silva Lobato, R. M. de Miranda, R. C. O. de Almeida, and J.

DOI:10.1088/1674-0068/22/03/275-284

C. Pinheiro, J. Mol. Model. **14**, 39 (2008).
[17] *Siemens*, *SHELXTL^{TM} Version 5 Reference Manual*; Madison, Wisconsin, USA: Siemens Energy & Automoation Inc., (1994).
[18] (a) D. S. Kim, R. G. Chang. X. Y. Shen, Y. P. Chen, and H. D. Sun. Phytochemistry, **31**, 697 (1992);
(b) A. D. Becke, J. Chem. Phys. **98**, 5648 (1993).
[19] C. Lee, W. Yang, and R. G. Parr, Phys. Rev. B **37**, 785 (1988).
[20] M. J. Frisch, G. W. Trucks, H. B. Schlegel, G. E. Scuseria, M. A. Robb, J. R. Cheeseman, J. A. Jr, Montgomery, T. Vreven, K. N. Kudin, J. C. Burant,J. M. Millam, S. S. Iyengar, J. Tomasi, V. Barone, B. Mennucci, M. Cossi, G. Scalmani, N. Rega, G. A. Petersson, H. Nakatsuji, M. Hada, M. Ehara, K. Toyota, R. Fukuda, J. Hasegawa, M. Ishida, T. Nakajima, Y. Honda, O. Kitao, H. Nakai, M. Klene, X. Li, J. E. Knox, H. P. Hratchian, J. B. Cross, C. Adamo, J. Jaramillo, R. Gomperts, R. E. Stratmann, O. Yazyev, A. J. Austin, R. Cammi, C. Pomelli, J. W. Ochterski, P. Y. Ayala, K. Morokuma, G. A. Voth, P. Salvador, J. J. Dannenberg, V. G. Zakrzewski, S. Dapprich, A. D. Daniels, M. C. Strain, O. Farkas, D. K. Malick, A. D. Rabuck, K. Raghavachari, J. B. Foresman, J. V. Ortiz, Q. Cui, A. G. Baboul, S. Clifford, J. Cioslowski, B. B. Stefanov, G. Liu, A. Liashenko, P. Piskorz, I. Komaromi, R. L. Martin, D. J. Fox, T. Keith, M. A. Al-Laham, C. Y. Peng, A. Nanayakkara, M. Challacombe, P. M. W. Gill, B. Johnson, W. Chen, M. W. Wong, C. Gonzalez, and J. A. Pople, *Gaussian* 03 (*Revision B*.01), Pittsburgh, PA: Gaussian, Inc., (2003).
[21] Y. H. Wang and Y. Z. Chen, J. Nat. Prod. **60**, 1161 (1997).
[22] Z. Na, B. Jiang, X. M. Niu, Z. W. Lin, C. M. Li, and H. D. Sun, Acta Bot. Sin. **44**, 477 (2002).
[23] M. Y. Gui, Y. Aoyagi, Y. R. Jin, X. W. Li, T. Hasuda, K. Takeya, and H. Excisanin, J. Nat. Prod. **67**, 373 (2004).
[24] L. Ding, G. A. Liu, L. Wang, K. Sun, and H. Q. Wang, Indian J. Chem. B: Med. Chem. **45**, 548 (2006).
[25] J. Lamotte-Brassrur, G. Dive, D. Dehareng, and J. M. Ghuysn, J. Theor. Biol. **145**, 183 (1900).
[26] G. Sachs, J. M. Shin, C. Briving, B. Wallmark, and S. Hersey, Annu. Rev. Pharmacol. Toxicol. **35**, 277 (1955).

DOI:10.1088/1674-0068/22/03/275-284